Acta Pharmaceutica Sinica B 2021;11(7):2070–2079

Chinese Pharmaceutical Association
Institute of Materia Medica, Chinese Academy of Medical Sciences

Acta Pharmaceutica Sinica B

www.elsevier.com/locate/apsb
www.sciencedirect.com

ORIGINAL ARTICLE

Enzyme-instructed hybrid nanogel/nanofiber oligopeptide hydrogel for localized protein delivery

Tianyue Jiang[a], Yudi Ma[a], Xiao Xu[b], Qingchun Ji[a], Mingxing Feng[a], Cheng Cheng[a], Yang Feng[b], Bingfang He[a,*], Ran Mo[b,*]

[a]*School of Pharmaceutical Sciences, Nanjing Tech University, Nanjing 211816, China*
[b]*State Key Laboratory of Natural Medicines, Jiangsu Key Laboratory of Drug Discovery for Metabolic Diseases, Center of Advanced Pharmaceuticals and Biomaterials, China Pharmaceutical University, Nanjing 210009, China*

Received 13 May 2020; received in revised form 6 August 2020; accepted 20 August 2020

KEY WORDS

Protein delivery;
Oligopeptide hydrogel;
Nanogel;
Enzymatic catalysis;
Cytochrome *c*;
Apoptosis;
Local administration;
Cancer therapy

Abstract Enzyme-catalysis self-assembled oligopeptide hydrogel holds great interest in drug delivery, which has merits of biocompatibility, biodegradability and mild gelation conditions. However, its application for protein delivery is greatly limited by inevitable degradation of enzyme on the encapsulated proteins leading to loss of protein activity. Moreover, for the intracellularly acted proteins, cell membrane as a primary barrier hinders the transmembrane delivery of proteins. The internalized proteins also suffer from acidic and enzymatic degradation in endosomes and lysosomes. We herein develop a protease-manipulated hybrid nanogel/nanofiber hydrogel for localized delivery of intracellularly acted proteins. The embedded polymeric nanogels (CytoC/aNGs) preserve activity of cytochrome *c* (CytoC) that is an intracellular activator for cell apoptosis as a model protein against proteolysis, and do not affect the gelation properties of the protease-catalysis assembled hydrogels. The injectable hydrogel (CytoC/aNGs/Gel) serves as a reservoir to enhance intratumoral retention and realize sustainable release of CytoC/aNGs. The released CytoC/aNGs increase cellular uptake of CytoC and enhance its intracellular delivery to its target site, cytoplasm, resulting in favorable apoptosis-inducing and cytotoxic effects. We show that a single local administration of CytoC/aNGs/Gel efficiently inhibit the tumor growth in the breast tumor mouse model.

*Corresponding authors.
E-mail addresses: bingfanghe@njtech.edu.cn (Bingfang He), rmo@cpu.edu.cn (Ran Mo).
Peer review under responsibility of Chinese Pharmaceutical Association and Institute of Materia Medica, Chinese Academy of Medical Sciences.

https://doi.org/10.1016/j.apsb.2020.11.010

1. Introduction

Protein therapeutics with high specific bioactivity have demonstrated their considerable potential for the treatment of many diseases including cancer[1,2]. However, a host of protein drugs and drug candidates have limitations that enormously hamper their exploitation and application, such as poor stability, vulnerable to enzymatic degradation and short half-life[2,3]. For the intracellularly acted proteins, cell membrane as a major barrier greatly impedes the delivery of proteins to their intracellular targets. To address these issues, micro- and nanotechnology-based drug delivery systems are increasingly being developed, such as polymeric micro/nanoparticles[4,5], nanogels[6,7], inorganic nanoparticles[8,9], microneedles[10,11], and hydrogels[12,13]. Hydrogels with high water capacity and porous structure offer a more benign environment for encapsulation of biologics, including proteins and cells[14].

Peptide hydrogels that are formed by self-assembly of nanofibers from short peptides (oligopeptides) open an avenue for the construction of semisolid biomaterials with good biocompatibility and biodegradability, which have extensively been applied for drug delivery[15,16] and tissue engineering[17,18]. Oligopeptide-based gelators assemble into nanofibers by non-covalent interactions, including H-bond, hydrophobic, electrostatic, $\pi-\pi$ stacking, and β-sheet interactions. Stimuli used for precursor-to-gelator formation contain temperature[19], pH[20,21], ionic strength[22,23], solvent polarity[24], and enzymatic catalysis[25,26]. Among them, enzymatic reaction provides unique region/enantio-selectivity for the hydrogel assembly, and has mild conditions, such as aqueous environment, neutral pH, and body temperature, which are favorable for fragile therapeutics, particularly for proteins.

The enzymes involved in manipulating the hydrogel assembly cover from protease[27,28], phosphatase[29,30], and transglutaminase[31,32], to lipase[33]. Proteases with numerous varieties and diverse specific recognition sites attract more and more attentions to induce the formation of hydrogels, such as thermolysin[34,35], matrix metalloproteinase[36,37], and thrombin[38]. However, application of protease-instructed self-assembled hydrogels for protein delivery is greatly restricted, since the proteases would inevitably digest the protein payloads leading to loss of protein activity. Meanwhile, for intracellularly acted proteins, they released from the hydrogel still suffer from delivery barriers, such as cell membrane and endocytotic vesicles[39]. Accordingly, it remains elusive for local delivery of intracellularly-acted proteins by the protease-instructed self-assembled oligopeptide hydrogels.

To this end, we developed a hybrid nanogel/hydrogel composite assembled by protease catalysis for local delivery of intracellularly active protein therapeutics (Fig. 1). Cytochrome *c* (CytoC) was selected as a model protein, which can activate caspases-dependent apoptosis by binding apoptotic protease activating factor-1 in the cytoplasm[40,41]. WQ9-2[42], a metalloprotease is chosen as a model protease, which can induce bond formation between the Fmoc-Phe (Fmoc-F) and Phe-Phe-Dopa (FF-Dopa) precursors. The synthesized Fmoc-FFF-Dopa hydrogelators self-assemble to form nanofiber-based hydrogel. However, WQ9-2 can degrade a variety of proteins owing to its broad substrate specificity (Fig. 1A). To protect CytoC against the WQ9-2-mediated hydrolysis during the hydrogelation process, CytoC was pre-loaded in polymeric nanogels (denoted as CytoC/aNGs) using emulsion polymerization. The nanogels provide a protective cage for CytoC from degradation by spatially hindering WQ9-2 to reach CytoC, and therefore preserve the activity and function of the encapsulated CytoC. Addition of the nanogels does not lead to any significant impairment on gel-forming properties. The hydrogel (denoted as CytoC/aNGs/Gel) can be acquired by a facile and gentle method, which is prepared by simply mixing the solution containing CytoC/aNGs and precursors with the WQ9-2 solution (Fig. 1A). Of note, the obtained CytoC/aNGs/Gel is injectable, which minimizes the burst release of *in situ* gelated hydrogels and avoids the implantation surgery of non-injectable hydrogels.

To pursue efficient delivery of CytoC to cytoplasm, 2-(dimethylamino)ethyl methacrylate (DMAEMA) monomer and glycerol dimethacrylate (GDA) crosslinker are used for preparation of CytoC/aNGs in addition to acrylamide (AAm). The acid-degradable GDA crosslinker enables CytoC/aNGs to release CytoC in acidic endo-lysosomes in a controllable manner, while the introduction of DMAEMA provides CytoC/aNGs with many tertiary amine groups for endo-lysosomal escape of the released CytoC by proton sponge effect[43]. The locally-injected CytoC/aNGs/Gel as a depot supports prolonged retention and sustainable drug release at the tumor site. The released CytoC/aNGs from the hydrogels increase cellular uptake of CytoC, liberate CytoC in the endo-lysosomes and promote transport of the released CytoC to the cytoplasm, therefore producing efficient apoptosis-inducing effect to suppress tumor growth (Fig. 1B).

2. Materials and methods

2.1. Materials

Fmoc-F and FF-Dopa were provided from GL Biochem Co., Ltd. (Shanghai, China). CytoC was purchased from Sigma−Aldrich LLC. (Shanghai, China). AAm, DMAEMA and *N*,*N*′-methylene bisacrylamide (MBA) were purchased from Aladdin Bio-Chem Technology Co., Ltd. (Shanghai, China). GDA was purchased from TCI Development Co., Ltd. (Shanghai, China). WQ9-2 from *Bacillus cereus* was expressed and purified as previously described[42].

2.2. Preparation and characterization of CytoC/aNGs

CytoC/aNGs were prepared by single emulsion method as previously described[44]. In brief, PBS (pH 7.4) containing CytoC (2 mg), AAm (45 mg), DMAEMA (25 mg) and GDA (15 mg) was added dropwise into 5 mL of hexane containing dioctyl sulfosuccinate sodium salt and Brij L4 under stirring for 10 min at 4 °C. Ammonium persulfate and tetramethylethylenediamine were added successively to initiate the polymerization. After 2 h of reaction, hexane was removed by evaporation, and the residuals were washed with absolute ethanol. CytoC/aNGs were obtained after vacuum drying. CytoC/aNGs were resuspended in PBS, dispersed by ultrasonication and washed by buffer exchange using ultrafiltration. The CytoC-loading capacity was ∼2%. The CytoC-encapsulated non-degradable nanogels (CytoC/nNGs) were prepared by AAm and MBA instead using the same method. The particle sizes of the nanogels were determined by zetasizer (Malvern, Nano ZS90, UK). The morphology was characterized by transmission electron microscope (TEM, Hitachi, HT7700, Japan).

The peroxidase activity was measured by 2,2′-azino-bis(3-ethylbenzthiazoline-6-sulfonic acid, ABTS) assay[45]. CytoC and CytoC/aNGs (1 mg/mL) were incubated with WQ9-2 (CytoC/WQ9-2, 5:1, *w*/*w*) for 0.5 h, respectively. 100 μL of the sample was then mixed with 400 μL of H_2O_2 (25 mmol/L) and 500 μL ABTS (1 mg/mL). The absorbance spectra of samples were recorded at 418 nm by microplate reader (Tecan, Infinite M1000 Pro, Switzerland). The untreated CytoC and CytoC/aNGs were taken as controls.

CytoC dissolved in the sodium bicarbonate buffer (50 mmol/L, pH 9) was reacted with rhodamine bisothiocyanate in DMSO (1:1, mol/mol) at 4 °C for 8 h. The solution was then dialyzed against water after 24 h. The rhodamine-labeled CytoC (Rho-CytoC) was obtained, and Rho-CytoC/aNGs were prepared. To assess the *in vitro* release of CytoC, Rho-CytoC/aNGs placed into a dialysis tube (50K MWCO) were incubated in the HEPES (10 mmol/L, pH 7.4) or acetate buffer (10 mmol/L, pH 5) at 37 °C over time, respectively. The Rho fluorescent intensity in the buffer was detected at $\lambda_{ex}/\lambda_{em}$ = 552/585 nm by microplate reader. Rho-CytoC/nNGs were taken as control. In addition, the released CytoC was analyzed by circular dichroism (CD) spectropolarimeter (Jasco, J-810, USA).

The pH-buffering capacity of CytoC/aNGs was assayed by acid titration method[46]. 5 mL of CytoC/aNGs (1 mg/mL) was adjusted to pH 10 by sodium hydroxide (0.3 mol/L). 40 μL aliquot of hydrochloric acid (0.02 mol/L) was then added into the CytoC/aNGs solution dropwise until reaching pH 4. The volume of added hydrochloric acid was recorded. CytoC/nNGs were taken as reference.

2.3. *Preparation and characterization of CytoC/aNGs/Gel*

800 μL of PBS (pH 7.4) containing CytoC/aNGs, Fmoc-F and FF-Dopa was mixed with 200 μL of WQ9-2, and then incubated for 4 h to obtain CytoC/aNGs/Gel. The final concentrations of CytoC and WQ9-2 were 1 and 0.2 mg/mL, respectively, while that of Fmoc-F and FF-Dopa were 10 and 20 mmol/L, respectively. The morphology of the hydrogel was characterized by TEM and scanning electron microscope (SEM, Hitachi, S4800N, Japan).

The rheology of CytoC/aNGs/Gel was studied. 1.6 mL of the solution containing CytoC/aNGs and precursors was placed on a parallel plate (50 mm diameter) with a gap of 0.8 mm. After addition of WQ9-2 (0.4 mL), dynamic time sweeps were recorded at 37 °C (frequency: 2 Hz, strain: 2%) by rheometer (Anton Paar, MCR302, Austria).

To investigate the *in vitro* release of the hydrogel, Rho-CytoC/aNGs/Gel was added into the bottom of the tube and left to stand for 1 h, followed by gentle addition of PBS on the top of the hydrogel. The tube was incubated at 37 °C in a shaker (Crystal, IS-RDV1, USA). The supernatant was collected after different time and replaced with fresh buffer. The fluorescence intensity of Rho-CytoC in the supernatant was detected at $\lambda_{ex}/\lambda_{em}$ = 552/585 nm by microplate reader.

2.4. *Cell culture*

Human breast cancer (MCF-7) cells provided by the Cell Bank of Chinese Academy of Sciences were cultured in DMEM containing fetal bovine serum (10%) at 37 °C with 5% CO_2.

2.5. *Cellular uptake*

MCF-7 cells were incubated with Rho-CytoC/aNGs and Rho-CytoC at 37 °C for different time, respectively. The cells were then washed by ice-cold PBS and disrupted by cell lysate, followed by centrifugation. The Rho fluorescence intensity in the supernatant was detected by microplate reader, while the concentration of cell proteins was quantified by BCA assay kit (Thermo Scientific).

2.6. *Endocytosis pathway*

MCF-7 cells were pre-incubated at 4 °C or in the presence of different endocytosis inhibitors, such as chlorpromazine (CPZ, 10 μmol/L), methyl-β-cyclodextrin (MCD, 3 mmol/L), amiloride (AMI, 1 mmol/L) and nystatin (NYS, 25 μg/mL) for 1 h, followed by incubation with Rho-CytoC/aNGs or Rho-CytoC/nNGs for additional 2 h. The cells were then washed by ice-cold PBS and disrupted by cell lysate, followed by centrifugation. The Rho fluorescence intensity and the concentration of cell proteins were determined, respectively. The cells incubated with the corresponding nanogels at 37 °C for 2 h were taken as control.

2.7. *Intracellular distribution*

MCF-7 cells were incubated with Rho-CytoC/aNGs and Rho-CytoC/nNGs at 37 °C for 1 and 4 h, respectively. The cells were then washed by ice-cold PBS, and further incubated with Lyso-Tracker Green (50 nmol/L) at 37 °C for 45 min. After washed by ice-cold PBS, the cells were observed by confocal microscope (Zeiss, LSM 700, Germany).

2.8. *Activation of apoptosis*

MCF-7 cells were incubated with CytoC, CytoC/nNGs and CytoC/aNGs (20 μg/mL) at 37 °C, respectively. The incubation time was 8 h for annexin V-FITC/PI (BD Pharmingen, USA) and active caspase 3 staining (Servicebio, China), and 18 h for TUNEL staining (Roche Life Science, Switzerland). The following procedures were performed according to the manufacturers' protocols. The cells were observed by fluorescent microscope (Olympus, IX51, Japan), and analyzed by flow cytometer (BD, Accuri C6, USA).

2.9. *In vitro cytotoxicity*

MCF-7 cells were incubated with CytoC, CytoC/nNGs, CytoC/aNGs, BSA/aNGs and blank aNGs at 37 °C for 24 h, respectively, and then incubated with methylthiazolyldiphenyl-tetrazolium bromide (0.5 mg/mL) for additional 4 h. The supernatant was removed and dimethyl sulfoxide was added. The absorbance of the solution was determined at 570 nm, and the cell viability was calculated.

2.10. *Animal and tumor mouse model*

All experimental procedures were executed according to the protocols approved by Nanjing Tech University Animal Care and Use Committee. BALB/c nude mice (female, 6 weeks) were provided by Qinglongshan Animal Center (Nanjing, China). The xenograft tumor mouse model was established as previously described[47]. The tumor length and width were measured by vernier caliper.

2.11. *In vivo tumor retention*

CytoC/aNGs was labeled with Cy5.5. In brief, CytoC/aNGs dissolved in the sodium bicarbonate buffer (pH 8.5) was added with Cy5.5 NHS ester (1:1, mol/mol). After reaction at 4 °C for 8 h, Cy5.5-CytoC/aNGs was obtained after repeated buffer exchange with PBS. The tumor-bearing mice were intratumorally administrated with Cy5.5-CytoC/aNGs/Gel or Cy5.5-CytoC/aNGs (5 mg/kg, 0.1 mL). The mice were imaged by *in vivo* imaging system (PerkinElmer, Lumina II, USA).

2.12. *In vivo antitumor activity*

MCF-7 tumor-bearing mice received a single intratumoral administration of CytoC, CytoC/aNGs and CytoC/aNGs/Gel (5 mg/kg, 0.1 mL), respectively. The tumor volume and body weight were measured every other day. The mice were euthanatized 14 days after administration. The tumors and normal tissue were harvested, and stained by hematoxylin and eosin (H&E) for the histological examination. The activated caspase 3 in the tumor was examined by immunofluorescence staining. The stained sections were imaged by microscope (Olympus).

2.13. *Immune response evaluation*

CytoC/aNGs/Gel (5 mg/kg, 0.1 mL) was subcutaneously injected into the normal mice. On the other hand, WQ9-2 (1 and 10 mg/kg) was intravenously injected into the normal mice. The blood samples were harvested after different time. The cytokines in the serum, such as tumor necrosis factor (TNF)-α, interleukin (IL)-1β, IL-6 and IL-10 were assayed by the corresponding ELISA kit (Cloud-Clone, USA).

3. Results and discussion

3.1. *Preparation and characterization of CytoC/aNGs/Gel*

CytoC/aNGs were prepared by single emulsion method, which consisted of a polymeric network shell by polymerization of AAm, DMAEMA and GDA. The obtained CytoC/aNGs had an average hydrodynamic diameter of ∼44 nm (Fig. 2A) and polydispersity index (PDI) of ∼0.208. CytoC/nNGs were prepared by AAm and MBA, a non-degradable crosslinker, which had a particle size of ∼38 nm (Supporting Information Fig. S1) and PDI of ∼0.224. To demonstrate the protective effect of aNGs on CytoC against the WQ9-2-mediated degradation, the activities of CytoC/aNGs in the absence and presence of WQ9-2 were determined by ABTS assay. CytoC/aNGs treated with WQ9-2 maintained a comparable activity to the untreated CytoC/aNGs (Supporting Information Fig. S2). However, the activity of the free CytoC incubated with WQ9-2 dramatically reduced to 33.1% of the untreated one, suggesting that WQ9-2 can rapidly degrade CytoC, leading to loss of its activity. These findings indicate that the polymeric shells of CytoC/aNGs impede spatially the encapsulated CytoC access to the WQ9-2 protease and therefore protect CytoC against enzymatic degradation.

We further evaluated the acid-triggered degradability of CytoC/aNGs by directly monitoring the morphologic variation under acidic condition. The TEM images showed that disruption of CytoC/aNGs was observed after incubation with acidic buffer solution (pH 5) for 12 h, while no significant change in the morphology of CytoC/nNGs incubated at the same condition (Supporting Information Fig. S3), suggesting that acidity, such as endo-lysosomal acidities, can trigger the cleavage of GDA accompanied by the disassembly of CytoC/aNGs. Subsequently, to demonstrate whether this acid-responsive dissociation of CytoC/aNGs could promote the release of CytoC, we determined the release profiles of Rho-CytoC from aNGs and nNGs at pH 7.4 and 5 by dialysis method, respectively. 53.1% of Rho-CytoC was released from aNGs at pH 5 compared with 13.5% at pH 7.4 within 24 h, while no significant difference in the release behavior of Rho-CytoC from nNGs between two pH values (Supporting Information Fig. S4). Moreover, the released CytoC was

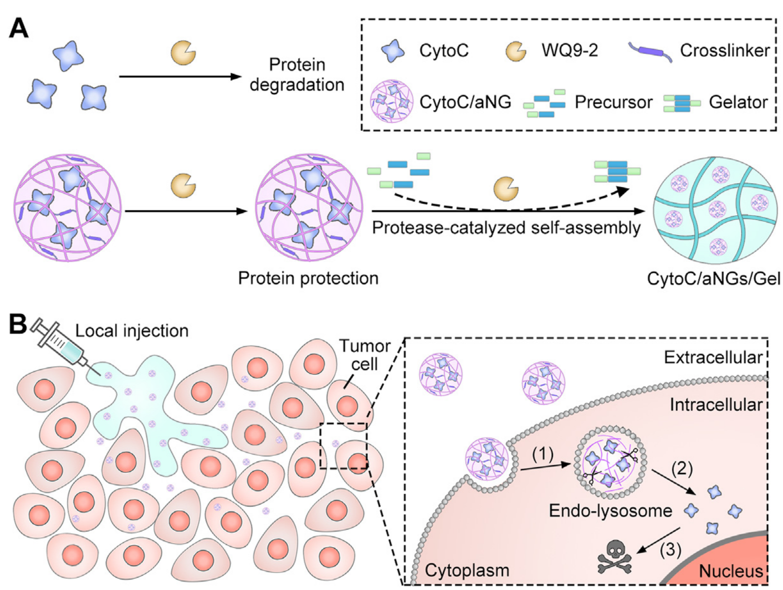

Figure 1 (A) Schematic diagram of preparation of CytoC/aNGs/Gel that was obtained by mixing CytoC/aNGs and precursors (Fmoc-F and FF-Dopa) with the WQ9-2 protease. (B) Schematic diagram of CytoC/aNGs/Gel as a drug depot for localized delivery of CytoC, which prolonged tumor retention and supported sustainable release of CytoC/aNGs. (1) The released aNGs from the hydrogel was endocytosed by the tumor cells, and responsively released encapsulated CytoC in the acidic endo-lyosomes; (2) the released CytoC transported into the cytoplasm by endo-lysosomal disruption caused by aNGs with the proton sponge effect; (3) CytoC in the cytoplasm activated the intrinsic apoptosis pathway to cause the tumor cell death.

collected, followed by respective examination *via* CD spectrum and ABTS assay. The CD spectrum of the released CytoC was consistent to that of the native CytoC (Supporting Information Fig. S5), deducing that the released CytoC has the similar secondary structure to the native one. The ABTS assay results showed that the released CytoC still remained its activity relative to the native CytoC (Supporting Information Fig. S6). These data suggest that there is no significant conformational variations and activity loss of CytoC in the encapsulation and release process. Taken together, the nanogel can hamper the enzymatic hydrolysis, preserve the activity of CytoC, and responsively disassemble under acidic environment to release the active CytoC.

CytoC/aNGs/Gel was obtained by WQ9-2-triggered self-assembly of oligopeptide precursors. The solution containing CytoC/aNGs and two precursors, the Fmoc-F and FF-Dopa peptides was added with WQ9-2 (Supporting Information Fig. S7). The hydrogel formation was investigated by detecting the rheology change of the solution (Fig. 2B). Upon addition of WQ9-2, noticeable elevation of the storage (G′) and loss moduli (G″) was observed over time. The G′ value increased to reach a plateau of $\sim 10^3$ Pa, which was about 10-fold that of the G″ value, indicating that the hydrogel is formed with a high mechanical strength. Incorporation of CytoC/aNGs was found to enhance the elasticity of hydrogel, as shown by a plateau with the higher G′ value, and to slow down the speed of hydrogel formation, as indicated by prolonged period of time reaching a plateau[48]. The morphology of the assembled CytoC/aNGs/Gel was visualized by TEM and SEM. The TEM images showed that CytoC/aNGs had spherical structures, while the hydrogel presented nanofiber architecture as elementary units (Fig. 2C). As shown in the TEM image of CytoC/aNGs/Gel, CytoC/aNGs were dispersed around the entangled nanofibrils of the hydrogel. The SEM image displayed that the lamellar structure formed by fiber bundles supported the structure of CytoC/aNGs/Gel, and a large number of CytoC/aNGs were encapsulated in the hydrogel (Fig. 2D).

To demonstrate that the hydrogel could serve as a reservoir for sustainable release of CytoC, we determined the release profiles of Rho-CytoC/aNGs from the hydrogel at pH 7.4 (Fig. 3A). A prolonged release of Rho-CytoC/aNGs was observed after Rho-CytoC/aNGs/Gel was incubated with PBS at pH 7.4, suggesting that the hydrogel could sustainably release Rho-CytoC/aNGs. In addition, the increased concentration of the peptide precursors leads to a slower release rate. This result indicates that the release rate of CytoC/aNGs from the hydrogel can be tuned on-demand by adjusting the monomer concentration. The DMAEMA monomer used for preparation of CytoC/aNGs contains tertiary amine group, which endows CytoC/aNGs with proton sponge effect for endosomal/lysosomal escape. To validate this, the pH-buffering capacity of CytoC/aNGs was evaluated by monitoring the pH value change after addition of acid (Fig. 3B). More volume of acid

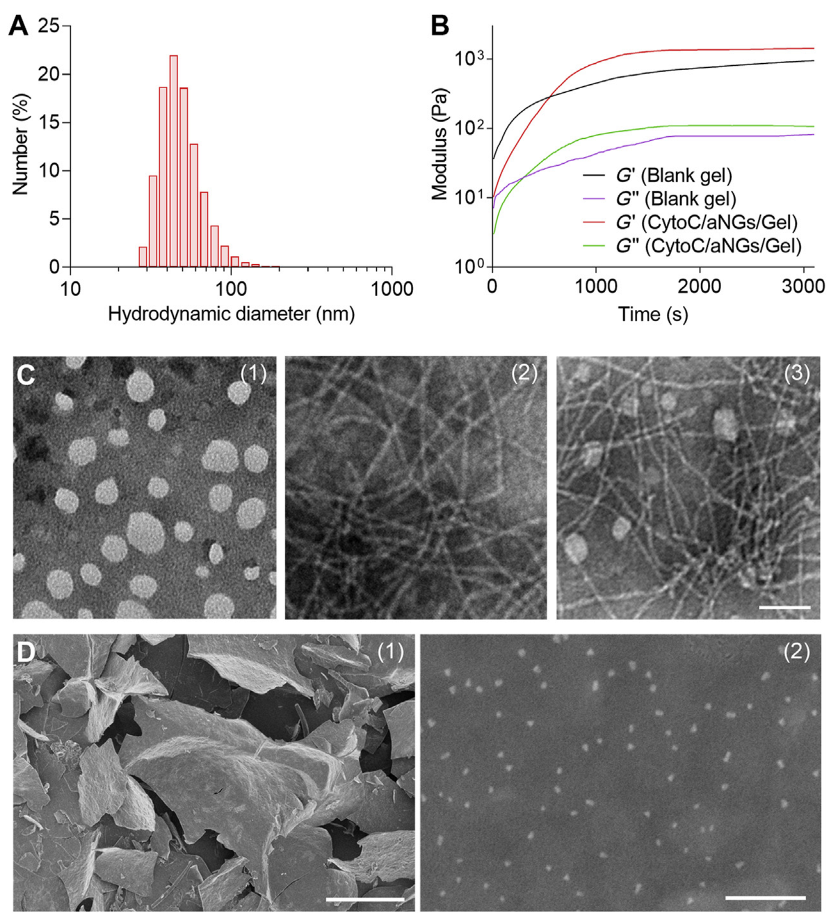

Figure 2 (A) Particle size distribution of CytoC/aNGs. (B) Changes in the moduli of the hydrogel after adding WQ9-2. (C) TEM images of CytoC/aNGs (1), blank hydrogel (2) and CytoC/aNGs/Gel (3). Scale bar = 80 nm. (D) SEM images of CytoC/aNGs/Gel at low (1) and high (2) magnification. Scale bars = 400 μm (1) and 400 nm (2).

was added to make the pH value of the solution containing CytoC/aNGs decrease from 7.4 to 4 compared with that of CytoC/nNGs, indicating the stronger pH-buffering ability of CytoC/aNGs containing numerous tertiary amine groups.

3.2. *Intracellular delivery and apoptosis-inducing effect*

We estimated the cellular uptake of CytoC/aNGs on MCF-7 cell model to demonstrate enhanced intracellular accumulation of CytoC delivered by aNGs (Fig. 3C). Incubation with Rho-CytoC/aNGs resulted in significantly higher fluorescent signals within MCF-7 cells at all the studied time points than incubation with the free Rho-CytoC, indicating that CytoC/aNGs are efficiently taken up by the cancer cells, which overcomes the cell membrane barrier to the native CytoC and increases its concentration within the cancer cells. Furthermore, the endocytosis pathway of the nanogels was explored by a competitive inhibition method. The uptake of either Rho-CytoC/aNGs or Rho-CytoC/nNGs by MCF-7 cells was compared with and without specific endocytosis inhibitors. The presence of CPZ markedly reduced intracellular fluorescent signals from both Rho-CytoC/aNGs and Rho-CytoC/nNGs compared with other inhibitors (Fig. 3D and Supporting Information Fig. S8), suggesting that both nanogels were internalized by MCF-7 cells *via* clathrin-mediated pathways[49,50]. Considering that CytoC/aNGs are entrapped in the endo-lysosomes after endocytosis and would be degraded by endo-lysosomal acidities and enzymes, we further evaluated the endo-lysosome-escaping potential of CytoC/aNGs. Intracellular

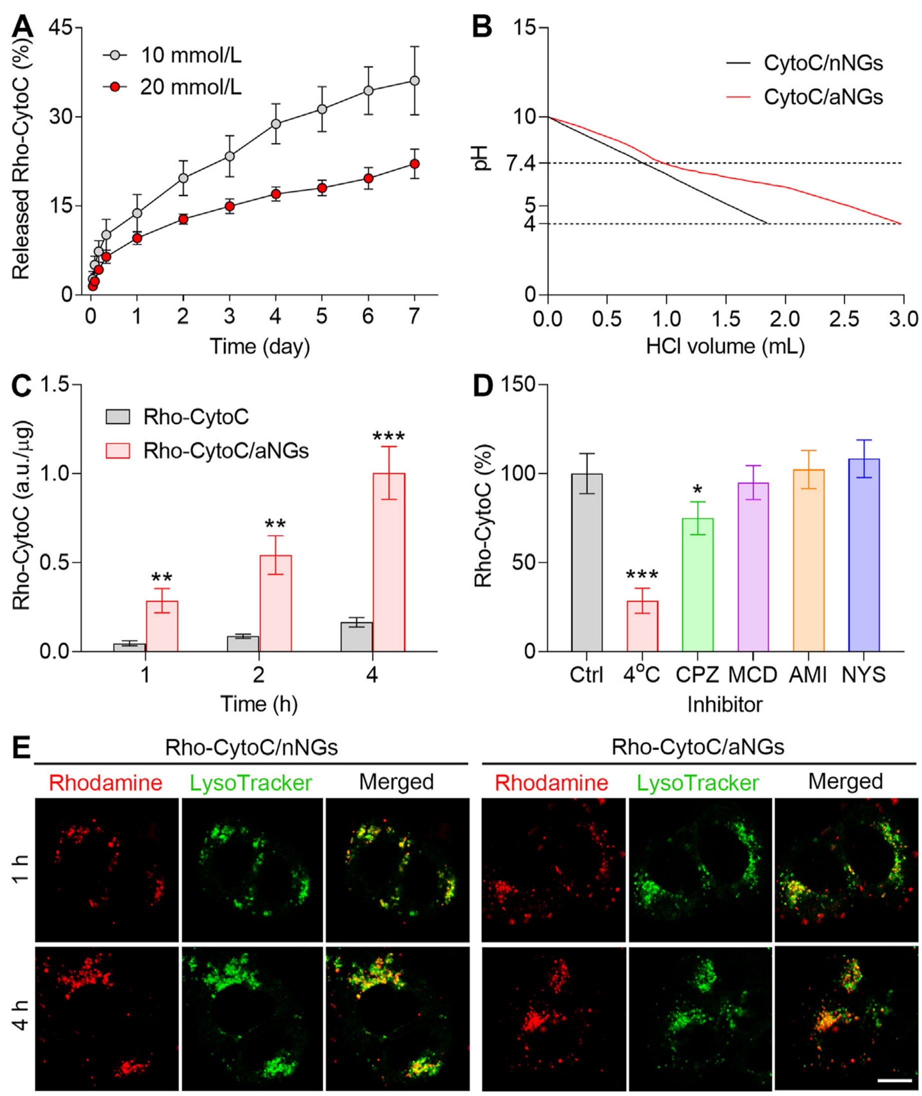

Figure 3 (A) *In vitro* protein release profiles of Rho-CytoC/aNGs/Gel at different concentration of the Fmoc-F precursor. Data are presented as mean ± SD ($n=3$). (B) Acid titration profiles of CytoC/aNGs and CytoC/nNGs. (C) Cellular uptake of Rho-CytoC/aNGs and Rho-CytoC on MCF-7 cells after incubation for different time. Data are presented as mean ± SD, $n=3$; $^{**}P < 0.01$, $^{***}P < 0.001$ *versus* Rho-CytoC. (D) Relative uptake efficiency of Rho-CytoC/aNGs on MCF-7 cells under different conditions. Ctrl, untreated control; CPZ, chlorpromazine; MCD, methyl-β-cyclodextrin; AMI, amiloride; NYS, nystatin. Data are presented as mean ± SD, $n=3$; $^{*}P < 0.05$, $^{***}P < 0.001$ *versus* Ctrl. (E) Intracellular distribution of Rho-CytoC/aNGs and Rho-CytoC/nNGs on MCF-7 cells after incubation for different time monitored by confocal microscope. Endo-lysosomes were stained by LysoTracker Green. Scale bar = 10 μm.

distribution of Rho-CytoC/aNGs was monitored within MCF-7 cells by confocal microscope (Fig. 3E). At 1 h post-incubation, a high proportion of the Rho fluorescent signals (red) of Rho-CytoC/aNGs were co-localized with that of endo-lysosomes (green) suggesting that the internalized CytoC/aNGs suffer from the endo-lysosomal entrapment. However, most of the Rho fluorescent signals were observed to be dissociated from the endo-lysosomal fluorescent signals after MCF-7 cells were incubated with Rho-CytoC/aNGs for 4 h. In a stark contrast, a large range of co-localization of the Rho and endo-lysosomal fluorescent signals was visualized in the Rho-CytoC/nNGs group at 4 h post-incubation. These results indicate that CytoC/aNGs can release CytoC in the acidic endo-lysosomes, and meanwhile, cause the endo-lysosomal disruption by the proton sponge effect to enable transportation of the released CytoC from endo-lysosomes to cytoplasm.

The apoptosis-inducing activities of CytoC/aNGs on MCF-7 cells were firstly assessed by annexin V-FITC/PI dual staining (Fig. 4A). The cancer cells treated with the free CytoC solution showed a limited apoptosis with a total apoptotic ratio of ~5.7%, which is attributed primarily to poor cell membrane permeability of CytoC. Treatment with CytoC/nNGs also led to only ~7.1% of cell apoptosis, which is due mainly to inefficient CytoC release and endo-lysosomal escape of CytoC/nNGs in spite of relatively higher cellular uptake. On the contrary, the total apoptotic ratio of CytoC/aNGs was ~26.5%, much higher than that of CytoC/nNGs. Accordingly, it is inferred that the combination of effective cellular uptake, CytoC release and intracellular delivery realized by aNGs potentiates the activities of CytoC on inducing cancer cell apoptosis. To further confirm the preferable apoptosis-inducing effects of CytoC/aNGs, activated caspase 3 and TUNEL assays were carried out, respectively (Fig. 4B). Activation of caspase-mediated cascade is a prerequisite for induction of apoptosis initiated by the cytoplasm distributed CytoC. As expected, the cancer cells after treatment with CytoC/aNGs exhibited an extensive expression

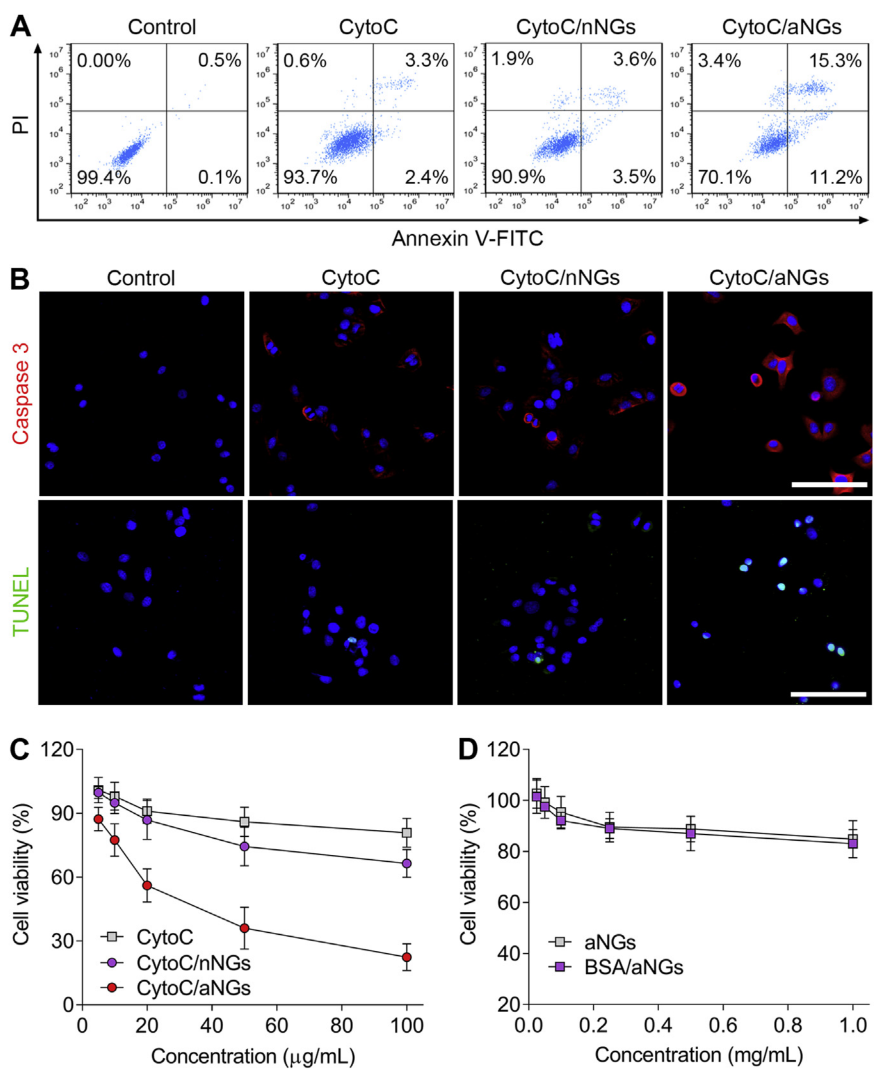

Figure 4 (A) Representative flow cytometric plots of MCF-7 cells after treatment with CytoC, CytoC/nNGs and CytoC/aNGs. The cells were dually stained by annexin V-FITC and PI. (B) Fluorescent images of MCF-7 cells after treatment with CytoC, CytoC/nNGs and CytoC/aNGs. The cells were stained by the active caspase 3 and TUNEL kits, respectively. Scale bar = 100 μm. (C) Viability of MCF-7 cells after 24 h of treatment with CytoC, CytoC/nNGs and CytoC/aNGs. Data are presented as mean ± SD, $n=5$. (D) Cell viability of MCF-7 cells after 24 h of treatment with the blank aNGs and BSA/aNGs. Data are presented as mean ± SD, $n=5$.

of activated caspase 3, a crucial executioner of apoptosis, while the amount of caspase 3 within the cells treated with either CytoC or CytoC/nNGs was extremely low. In addition, the fragmentation of the nucleosome occurs during cell apoptosis. Such signature apoptotic feature of massive DNA fragmentation stained by the TUNEL assay was observable in the cancer cells treated with CytoC/aNGs, compared with the negligible apoptosis characteristics after treatment with both CytoC and CytoC/nNGs. These results further confirmed elevation of cancer cell apoptosis induced by CytoC/aNGs.

Subsequently, we appraised the *in vitro* cytotoxicity of CytoC/aNGs toward MCF-7 cells (Fig. 4C). The dose-dependent increase in the cytotoxicity of CytoC/aNGs against the cancer cells was observed after 24 h of incubation. The half maximal inhibitory concentration was calculated to be 28.9 μg/mL. By comparison, neither CytoC nor CytoC/nNGs exhibited efficient cytotoxicity. The viabilities were higher than 60% in both CytoC- and CytoC/nNG-treated cancer cells at all the studied concentration. In addition, the blank aNGs without CytoC and bovine serum albumin loaded nanogels (BSA/aNGs) displayed negligible toxic effects on MCF-7 cells (Fig. 4D).

3.3. *In vivo tumor retention and antitumor efficacy*

To demonstrate the prolonged intratumoral retention of CytoC with the assistance of the hydrogel, the *in vivo* retention of Cy5.5-CytoC/aNGs/Gel in the tumor was estimated. The MCF-7 tumor-bearing mice were intratumorally administrated by Cy5.5-CytoC/aNGs and Cy5.5-CytoC/aNGs/Gel, respectively. Change in the fluorescent signal of Cy5.5 was monitored within a long period time (Fig. 5A). In the Cy5.5-CytoC/aNGs/Gel group, the fluorescent signal of Cy5.5 sustained in the tumor tissue within 4 days after local injection, and there was still a high Cy5.5 fluorescent signal as time increased to 8 days. In a sharp contrast, the intratumorally-injected Cy5.5-CytoC/aNGs showed noticeably reduction in the Cy5.5 fluorescent signal within 4 days, and very weak signal was detectable at 8 days post-injection. These data suggest that the oligopeptide hydrogel as a semisolid depot brings about dramatically prolonged retention time of CytoC/aNGs at the tumor site, which would render a long-term antitumor effect produced by CytoC.

To substantiate the feasibility of CytoC/aNGs/Gel for cancer treatment *in vivo*, the antitumor efficacy of CytoC/aNGs/Gel

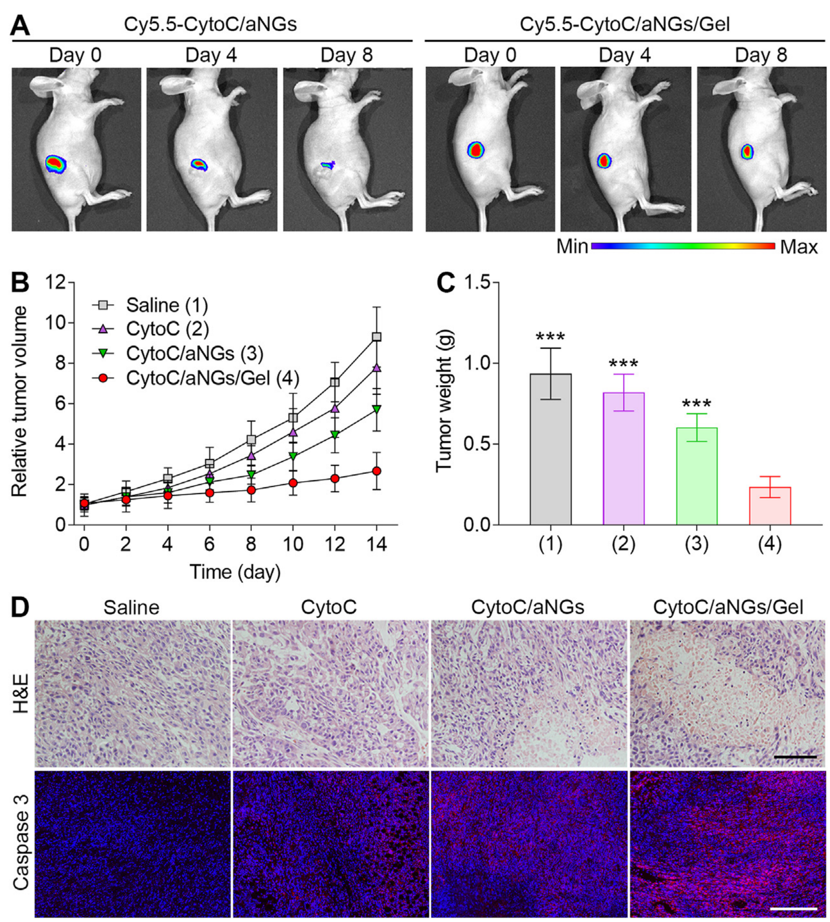

Figure 5 (A) *In vivo* imaging of the MCF-7 tumor-bearing mice after intratumoral injection of Cy5.5-CytoC/aNGs and Cy5.5-CytoC/aNGs/Gel. (B) Relative tumor volume of the MCF-7 tumor-bearing mice after a single intratumoral injection of saline, CytoC, CytoC/aNGs and CytoC/aNGs/Gel ($n = 6$ mice per group). (C) Weight of the tumors harvested from the mice at 14 days post injection of saline, CytoC, CytoC/aNGs and CytoC/aNGs/Gel ($n = 6$ mice per group). $^{***}P < 0.001$ *versus* CytoC/aNGs/Gel. (D) Representative images of the tumor sections stained by H&E and immunofluorescence at 14 days post injection of saline, CytoC, CytoC/aNGs and CytoC/aNGs/Gel. Scale bars = 100 μm (upper) and 200 μm (lower).

was assessed on the mouse models of xenograft MCF-7 tumors. Tumor growth was suppressed to different extent after a single intratumoral administration of various CytoC formulations including the CytoC solution, CytoC/aNGs solution and CytoC/aNGs/Gel, compared to saline as a negative control (Fig. 5B). CytoC/aNGs produced a higher effect on tumor inhibition than CytoC, which results mainly from improved intracellular delivery of CytoC provided by aNGs. More significantly, CytoC/aNGs/Gel exhibited a dominant effect on inhibiting tumor growth than the CytoC/aNGs solution, validating that the prolonged intratumoral retention and sustained release of CytoC/aNGs actualized by the oligopeptide hydrogel allow CytoC to produce a long-term antitumor effect. The lowest tumor weight from the mice was determined in the CytoC/aNGs/Gel treatment group 14 days after a single administration (Fig. 5C). The inhibitory ratio of CytoC/aNGs/Gel was 74.9%, significantly higher than 35.7% of the Cyto/aNGs solution. During the treatment with CytoC/aNGs/Gel, the mice did not display any significant body weight change (Supporting Information Fig. S9). Remission of massive tumor cells after the CytoC/aNGs/Gel treatment was examined by H&E staining. Moreover, the immunofluorescence images displayed the highest level of activated caspase 3 indicating cell apoptosis in the tumor harvested from the mice receiving CytoC/aNGs/Gel (Fig. 5D). There were no significant pathological changes observed in the normal tissues after the CytoC/aNGs/Gel treatment (Supporting Information Fig. S10). We also performed safety evaluation about immune response of the oligopeptide hydrogel-based formulation. A single subcutaneous injection of CytoC/aNGs/Gel did not cause any noticeable variation in the serum concentrations of typical inflammatory factors (Supporting Information Fig. S11). Moreover, no significant changes in the concentration of these inflammatory factors were determined after intravenous injection of WQ9-2 at the studied dosages (Supporting Information Fig. S12).

4. Conclusions

In conclusion, we developed a hybrid nanogel/nanofiber hydrogel for localized delivery of cytoplasm-targeted apoptotic protein, CytoC. aNGs preserved the activity of CytoC against degradation caused by WQ9-2, which catalyzed the bond-forming reaction between the peptide precursors for assembly of the hydrogel. The obtained hydrogel served as a CytoC storehouse to enhance intratumoral retention and realize sustainable release of CytoC/aNGs. CytoC/aNGs increased cellular uptake of CytoC and promoted its intracellular delivery to the target site, cytoplasm, leading to favorable apoptosis-inducing and cytotoxic effects. We showed that CytoC/aNGs/Gel efficiently inhibit tumor growth upon a single intratumoral administration. We also envision that this formulation design, as a promising strategy, has the potential of wide application in the delivery of other intracellularly-acted protein therapeutics for long-term disease management.

Acknowledgments

This work was supported by the National Key Research and Development Program of China (No. 2019YFA0905200), the National Natural Science Foundation of China (No. 81971730, No. 81503012), the Natural Science Foundation of Jiangsu Province of China for Excellent Young Scholars (No. BK20190084), the Young Elite Scientists Sponsorship Program by CAST (China).

Author contributions

Tianyue Jiang, Bingfang He and Ran Mo designed the research. Tianyue Jiang, Yudi Ma, Xiao Xu, Qingchun Ji, Mingxing Feng, Cheng Cheng and Yang Feng performed the experiments. Tianyue Jiang, Yudi Ma, Bingfang He and Ran Mo analyzed the data. Tianyue Jiang, Bingfang He and Ran Mo wrote the manuscript. All of the authors have read and approved the final manuscript.

Conflicts of interest

The authors have no conflicts of interest to declare.

Appendix A. Supporting information

Supporting data to this article can be found online at https://doi.org/10.1016/j.apsb.2020.11.010.

References

1. Walsh G. Biopharmaceutical benchmarks 2010. *Nat Biotechnol* 2010;**28**:917−24.
2. Leader B, Baca QJ, Golan DE. Protein therapeutics: a summary and pharmacological classification. *Nat Rev Drug Discov* 2008;**7**:21−39.
3. Wagner AM, Gran MP, Peppas NA. Designing the new generation of intelligent biocompatible carriers for protein and peptide delivery. *Acta Pharm Sin B* 2018;**8**:147−64.
4. Broaders KE, Grandhe S, Frechet JM. A biocompatible oxidation-triggered carrier polymer with potential in therapeutics. *J Am Chem Soc* 2011;**133**:756−8.
5. Kim SK, Foote MB, Huang L. The targeted intracellular delivery of cytochrome *c* protein to tumors using lipid-apolipoprotein nanoparticles. *Biomaterials* 2012;**33**:3959−66.
6. Liu M, Shen SY, Wen D, Li MR, Li T, Chen XJ, et al. Hierarchical nanoassemblies-assisted combinational delivery of cytotoxic protein and antibiotic for cancer treatment. *Nano Lett* 2018;**18**:2294−303.
7. Li S, Zhang J, Deng C, Meng FH, Yu L, Zhong ZY. Redox-sensitive and intrinsically fluorescent photoclick hyaluronic acid nanogels for traceable and targeted delivery of cytochrome *c* to breast tumor in mice. *ACS Appl Mater Interfaces* 2016;**8**:21155−62.
8. Zhang BL, Luo Z, Liu JJ, Ding XW, Li JH, Cai KY. Cytochrome *c* end-capped mesoporous silica nanoparticles as redox-responsive drug delivery vehicles for liver tumor-targeted triplex therapy *in vitro* and *in vivo*. *J Control Release* 2014;**192**:192−201.
9. Mendez J, Morales Cruz M, Delgado Y, Figueroa CM, Orellano EA, Morales M, et al. Delivery of chemically glycosylated cytochrome *c* immobilized in mesoporous silica nanoparticles induces apoptosis in HeLa cancer cells. *Mol Pharm* 2014;**11**:102−11.
10. Wang C, Ye YQ, Hochu GM, Sadeghifar H, Gu Z. Enhanced cancer immunotherapy by microneedle patch-assisted delivery of anti-PD1 antibody. *Nano Lett* 2016;**16**:2334−40.
11. Ye YQ, Wang JQ, Hu QY, Hochu GM, Xin HL, Wang C, et al. Synergistic transcutaneous immunotherapy enhances antitumor immune responses through delivery of checkpoint inhibitors. *ACS Nano* 2016;**10**:8956−63.
12. Liang YK, Kiick KL. Liposome-cross-linked hybrid hydrogels for glutathione-triggered delivery of multiple cargo molecules. *Biomacromolecules* 2016;**17**:601−14.
13. Lee F, Chung JE, Kurisawa M. An injectable hyaluronic acid−tyramine hydrogel system for protein delivery. *J Control Release* 2009;**134**:186−93.

14. Vermonden T, Censi R, Hennink WE. Hydrogels for protein delivery. *Chem Rev* 2012;**112**:2853−88.
15. Koutsopoulos S, Zhang SG. Two-layered injectable self-assembling peptide scaffold hydrogels for long-term sustained release of human antibodies. *J Control Release* 2012;**160**:451−8.
16. Zhao XY, Liu XY, Zhang PC, Liu YR, Ran W, Cai Y, et al. Injectable peptide hydrogel as intraperitoneal triptolide depot for the treatment of orthotopic hepatocellular carcinoma. *Acta Pharm Sin B* 2019;**9**: 1050−60.
17. Galler KM, Hartgerink JD, Cavender AC, Schmalz G, D'Souza RN. A customized self-assembling peptide hydrogel for dental pulp tissue engineering. *Tissue Eng* 2012;**18**:176−84.
18. Cheng TY, Chen MH, Chang WH, Huang MY, Wang TW. Neural stem cells encapsulated in a functionalized self-assembling peptide hydrogel for brain tissue engineering. *Biomaterials* 2013;**34**:2005−16.
19. Collier JH, Hu BH, Ruberti JW, Zhang J, Shum P, Thompson DH, et al. Thermally and photochemically triggered self-assembly of peptide hydrogels. *J Am Chem Soc* 2001;**123**:9463−4.
20. Ghosh A, Dobson ET, Buettner CJ, Nicholl MJ, Goldberger JE. Programming pH-triggered self-assembly transitions *via* isomerization of peptide sequence. *Langmuir* 2014;**30**:15383−7.
21. Zimenkov Y, Dublin SN, Ni R, Tu RS, Breedveld V, Apkarian RP, et al. Rational design of a reversible pH-responsive switch for peptide self-assembly. *J Am Chem Soc* 2006;**128**:6770−1.
22. Koutsopoulos S, Unsworth LD, Nagai Y, Zhang SG. Controlled release of functional proteins through designer self-assembling peptide nanofiber hydrogel scaffold. *Proc Natl Acad Sci U S A* 2009;**106**: 4623−8.
23. Zou RF, Wang Q, Wu JC, Wu JX, Schmuck C, Tian H. Peptide self-assembly triggered by metal ions. *Chem Soc Rev* 2015;**44**:5200−19.
24. Hashemnejad SM, Kundu S. Probing gelation and rheological behavior of a self-assembled molecular gel. *Langmuir* 2017;**33**:7769−79.
25. Gao Y, Shi JF, Yuan D, Xu B. Imaging enzyme-triggered self-assembly of small molecules inside live cells. *Nat Commun* 2012;**3**:1033.
26. Zhou J, Du XW, Chen XY, Wang JQ, Zhou N, Wu DF, et al. Enzymatic self-assembly confers exceptionally strong synergism with NF-kappaB targeting for selective necroptosis of cancer cells. *J Am Chem Soc* 2018;**140**:2301−8.
27. Conte MP, Sahoo JK, Abul-Haija YM, Lau KHA, Ulijn RV. Biocatalytic self-assembly on magnetic nanoparticles. *ACS Appl Mater Interfaces* 2018;**10**:3069−75.
28. Pappas CG, Sasselli IR, Ulijn RV. Biocatalytic pathway selection in transient tripeptide nanostructures. *Angew Chem Int Ed* 2015;**54**: 8119−23.
29. Liang CH, Zheng DB, Shi F, Xu TY, Yang CH, Liu JF, et al. Enzyme-assisted peptide folding, assembly and anti-cancer properties. *Nanoscale* 2017;**9**:11987−93.
30. Huang P, Gao Y, Lin J, Hu H, Liao HS, Yan XF, et al. Tumor-specific formation of enzyme-instructed supramolecular self-assemblies as cancer theranostics. *ACS Nano* 2015;**9**:9517−27.
31. Chen CX, Zhang Y, Fei R, Cao CH, Wang M, Wang JX, et al. Hydrogelation of the short self-assembling peptide I3QGK regulated by transglutaminase and use for rapid hemostasis. *ACS Appl Mater Interfaces* 2016;**8**:17833−41.
32. Bai JK, Chen CX, Wang JX, Zhang Y, Cox H, Zhang J, et al. Enzymatic regulation of self-assembling peptide A9K2 nanostructures and hydrogelation with highly selective antibacterial activities. *ACS Appl Mater Interfaces* 2016;**8**:15093−102.
33. Chronopoulou L, Lorenzoni S, Masci G, Dentini M, Togna AR, Togna G, et al. Lipase-supported synthesis of peptidic hydrogels. *Soft Matter* 2010;**6**:2525−32.
34. Toledano S, Williams RJ, Jayawarna V, Ulijn RV. Enzyme-triggered self-assembly of peptide hydrogels *via* reversed hydrolysis. *J Am Chem Soc* 2006;**128**:1070−1.
35. Williams RJ, Smith AM, Collins R, Hodson N, Das AK, Ulijn RV. Enzyme-assisted self-assembly under thermodynamic control. *Nat Nanotechnol* 2009;**4**:19−24.
36. Yang ZM, Ma M, Xu B. Using matrix metalloprotease-9 (MMP-9) to trigger supramolecular hydrogelation. *Soft Matter* 2009;**5**: 2546−8.
37. Tanaka A, Fukuoka Y, Morimoto Y, Honjo T, Koda D, Goto M, et al. Cancer cell death induced by the intracellular self-assembly of an enzyme-responsive supramolecular gelator. *J Am Chem Soc* 2015;**137**: 770−5.
38. Bremmer SC, Chen J, McNeil AJ, Soellner MB. A general method for detecting protease activity *via* gelation and its application to artificial clotting. *Chem Commun* 2012;**48**:5482−4.
39. Gu Z, Biswas A, Zhao MX, Tang Y. Tailoring nanocarriers for intracellular protein delivery. *Chem Soc Rev* 2011;**40**:3638−55.
40. Zhivotovsky B, Orrenius S, Brustugun OT, Doskeland SO. Injected cytochrome *c* induces apoptosis. *Nature* 1998;**391**:449−50.
41. Liu XS, Kim CN, Yang J, Jemmerson R, Wang XD. Induction of apoptotic program in cell-free extracts: requirement for dATP and cytochrome *c*. *Cell* 1996;**86**:147−57.
42. Xu JX, Jiang M, Sun HL, He BF. An organic solvent-stable protease from organic solvent-tolerant *Bacillus cereus* WQ9-2: purification, biochemical properties, and potential application in peptide synthesis. *Bioresour Technol* 2010;**101**:7991−4.
43. Lale SV, Kumar A, Naz F, Bharti AC, Koul V. Multifunctional ATRP based pH responsive polymeric nanoparticles for improved doxorubicin chemotherapy in breast cancer by proton sponge effect/endo-lysosomal escape. *Polym Chem* 2015;**6**:2115−32.
44. Cohen JA, Beaudette TT, Tseng WW, Bachelder EM, Mende I, Engleman EG, et al. T-cell activation by antigen-loaded pH-sensitive hydrogel particles *in vivo*: the effect of particle size. *Bioconjugate Chem* 2009;**20**:111−9.
45. Dutta K, Hu D, Zhao B, Ribbe AE, Zhuang JM, Thayumanavan S. Templated self-assembly of a covalent polymer network for intracellular protein delivery and traceless release. *J Am Chem Soc* 2017;**139**: 5676−9.
46. Mo R, Sun Q, Xue JW, Li N, Li WY, Zhang C, et al. Multistage pH-responsive liposomes for mitochondrial-targeted anticancer drug delivery. *Adv Mater* 2012;**24**:3659−65.
47. Mo R, Jiang TY, Gu Z. Enhanced anticancer efficacy by ATP-mediated liposomal drug delivery. *Angew Chem Int Ed* 2014;**53**: 5815−20.
48. Johnson SB, Dunstan DE, Franks GV. Rheology of cross-linked chitosan−alumina suspensions used for a new gelcasting process. *J Am Ceram Soc* 2002;**85**:1699−705.
49. Jiang TY, Mo R, Bellotti A, Zhou JP, Gu Z. Gel−liposome-mediated co-delivery of anticancer membrane-associated proteins and small-molecule drugs for enhanced therapeutic efficacy. *Adv Funct Mater* 2014;**24**:2295−304.
50. Zhang XX, Allen PG, Grinstaff M. Macropinocytosis is the major pathway responsible for DNA transfection in CHO cells by a charge-reversal amphiphile. *Mol Pharm* 2011;**8**:758−66.